Biomedical Research (Tokyo) **41** (2) 81–90, 2020

Low-vacuum scanning electron microscopy may allow early diagnosis of human renal transplant antibody-mediated rejection

Hiroki Yokoyama[1], Shinichi Okada[1], Yuko Yamada[1], Koichi Kitamoto[1], Sumire Inaga[2], Hironobu Nakane[2], Toshiyuki Kaidoh[2], Kazuho Honda[3], Susumu Kanzaki[1], and Noriyuki Namba[1]

[1] Division of Pediatrics and Perinatology, Faculty of Medicine, Tottori University, Japan; [2] Department of Anatomy, Faculty of Medicine, Tottori University, Japan; and [3] Department of Anatomy, Showa University School of Medicine, Japan

(Received 2 December 2019; and accepted 26 December 2019)

ABSTRACT

Antibody-mediated rejection (ABMR) is an important cause of both short- and long-term injury to renal allografts. Transplant glomerulopathy (TG) is strongly associated with ABMR and reduced graft survival. Ultrastructural changes in early-stage ABMR include TG as a duplication of the glomerular basement membrane (GBM), which can be observed only by transmission electron microscopy (TEM). Low-vacuum scanning electron microscopy (LVSEM) is a new technique that allows comparatively inexpensive, rapid, and convenient observations with high magnification. We analyzed human renal transplants using LVSEM and evaluated the ultrastructural changes representing TG in ABMR. GBM duplication was more clearly visible in the LVSEM images than in the light microscopy (LM) images. In the ABMR group, the cg score of the Banff classification was higher in 54% (7/13) of specimens for LVSEM images than for LM images. And 4 specimens exhibited duplication of the GBM analyzed by LVSEM, but not by LM. In addition, three-dimensional ultrastructural changes, such as coarse meshwork structures of GBM, were observed in ABMR specimens. The ABMR group also exhibited ultrastructural changes in the peritubular capillary basement membranes. In conclusion, analyses of renal transplant tissues using LVSEM allows the identification of GBM duplication and ultrastructural changes of basement membranes at the electron microscopic level, and is useful for early-stage diagnosis of ABMR.

Antibody-mediated rejection (ABMR) remains the most important barriers to successful renal transplantation. Despite advances in molecular biology and gene rearrangement, ABMR diagnosis remains dependent on histological findings (5). Transplant glomerulopathy (TG) is histological changes resulting from chronic vascular endothelial dysfunction caused by antibody-mediated injury (8). TG is defined by the presence of duplication of glomerular basement membrane (GBM), and strongly correlated with ABMR and renal transplant prognosis (6).

Observations by transmission electron microscopy (TEM) are important in diagnosing early-stage ABMR, since TG develops in stages best observed by TEM. These stages have been related to ABMR in recent studies (6, 21). Peritubular capillary (PTC) basement membrane multilayering is also an important early-stage ABMR finding observable by TEM (13, 19). The accurate diagnosis of early-stage ABMR is clinically important because TG is considered irreversible after they progress to a stage observable by light microscopy (LM) (8, 20). Early detection by TEM and treatment may help to prolong graft survival. Based on these findings, the Banff criteria were modified to include TG detectable only by electron microscopy (7, 14). The quantitative criteria in Banff 2015 for double contours, namely, the cg

Address correspondence to: Hiroki Yokoyama, MD
Division of Pediatrics and Perinatology, Faculty of Medicine, Tottori University,
36-1 Nishi-cho, Yonago City, Tottori, Japan
Tel: +81-859-38-6557, Fax: +81-859-38-6559
E-mail: hirokiy@Tottori-u.ac.jp

Table 1 *Quantitative criteria for double contour: cg score in Banff 2015 (14)*

cg0	No GBM double contours by light microscopy or EM
cg1a	No GBM double contours by light microscopy but GBM double contours in at least 3 glomerular capillaries by EM, with associated endothelial swelling and/or subendothelial electron-lucent widening
cg1b	Double contours of the GBM in 1–25% of capillary loops in the most affected nonsclerotic glomerulus by light microscopy; EM confirmation is recommended if EM is available
cg2	Double contours affecting 26–50% of peripheral capillary loops in the most affected glomerulus
cg3	Double contours affecting >50% of peripheral capillary loops in the most affected glomerulus

score is shown in Table 1. Although duplications of GBM are visible by LM in Banff code cg1b, they are visible only by electron microscopy in cg1a. ABMR will be underdiagnosed if pathologists rely on LM alone for assessment (12). Although currently "electron microscopy" refers only to TEM, there is issue that TEM is costly and time consuming. It is impossible to utilizing TEM for every case of renal transplant biopsy.

We recently reported the usefulness of low vacuum scanning electron microscopy (LVSEM) for the rapid three-dimensional analysis of renal biopsy specimens (11, 15, 16). LVSEM is comparatively less expensive, and it can facilitate convenient and quick observations because it does not require preliminary processing. A standard paraffin section of a tissue sample can be observed at high resolution at a range of magnifications for any part of interest within the section. The GBMs could be visualized by periodic acid methenamine silver (PAM) staining, and by using the backscattered electron (BSE) mode of LVSEM, because the PAM stain contains silver, a heavy metal, which enhances the backscattered electron signals. If ultrastructural pathological changes in ABMR, which at present are only identifiable using TEM, can be observed by LVSEM, the diagnosis of early-stage ABMR would be advanced significantly.

In this study, we assessed the utility of LVSEM in identifying ABMR, especially TG. We used LVSEM to analyze renal transplant specimens with and without (intraoperative 0-h biopsy controls) ABMR, focusing on the glomerular and peritubular capillaries, particularly GBM duplication.

MATERIALS AND METHODS

Among the renal transplant specimens that were pathologically diagnosed at Tottori University (283 individuals, 358 specimens) between January 2000 and December 2010, we selected seven patients with a Banff cg score ≥1 who were histopathologically diagnosed with ABMR (ABMR group). ABMR diagnoses in this study were ordered by specialists in renal transplant pathology using light microscopic findings and medical histories. Among these, past renal biopsy specimens existed in four patients (ABMR1–4), who were therefore included in the observation (13 specimens in total). In the ABMR group, no diagnoses or medical histories that denied ABMR after the renal biopsy were found as far as we could trace. In the control group, we extracted four cases for which special findings were not found on LM examinations of renal transplant intraoperative 0-h biopsies from the cases stored by the university. Control group samples were also checked to ensure that the donor had no history of renal diseases. No samples had available donor-specific antibody and complement fragment 4d (C4d) staining information which are regarded as marker to diagnose ABMR. TEM observation was not employed in all specimens when they were pathologically diagnosed. This research was conducted with the approval of the Ethics Committee of Tottori University (Permission No. 17A236).

The specimens used for LVSEM observations were prepared as described previously (11). Briefly, 5-μm-thick renal biopsy paraffin sections were used. Deparaffinized sections mounted on slides were stained with PAM for each case. PAM staining was performed using the conventional method for LM observations, but without the final H&E staining. The stained sections on the slides were directly observed and photographed using a Hitachi LVSEM (Miniscope TM-3030Plus; Hitachi Co., Ltd., Tokyo, Japan) at a pressure of 30 Pa and an acceleration voltage of 15 kV in the charge-up-reduction BSE mode.

Table 2 *Cases and Banff cg scores of this study*

case	specimen	post transplant	cg score LM	cg score LVSEM	Figure
ABMR-1	1-1	12 months	0	0	
	1-2	110 months	2	3	
ABMR-2	2-1	9 months	0	1a	
	2-2	14 months	0	1a	3a–f, 6a
	2-3	20 months	1b	1b	
ABMR-3	3-1	1 month	0	0	
	3-2	2 months	0	1a	6b, c
	3-3	4 months	1b	1b	
ABMR-4	4-1	1 month	0	1a	
	4-2	3 months	1b	2	
ABMR-5	5	180 months	2	2	
ABMR-6	6	12 months	2	3	2a–f 5a–d
ABMR-7	7	108 months	1b	1b	
		donor's age	cg score LM	cg score LVSEM	Figure
control-1		35y	0	0	
control-2		46y	0	0	1a–f
control-3		ND	0	0	
control-4		56y	0	0	

In this study, the GBM and the PTC basement membranes were observed primarily by PAM staining. Specimens were assessed as a whole at low power (×40). After observing the whole glomerulus in a specimen at ×400–600, the magnification was increased to ×1000, and a sequence of images was collected while moving the field of view clockwise from the 12 : 00 position. GBM, PTCs, and cells and their substructures were observed from low magnification to the maximum magnification (×10,000). The duplication of the GBM of each specimen was evaluated, and cg scoring was implemented by LM and LVSEM using the 2015 Banff classification as a reference.

Two samples from the ABMR group (ABMR2-2 and ABMR3-2) for which duplication of the GBM was not visible by LM were examined using the re-embedding TEM method. The paraffin-embedded specimens were deparaffinized in xylene and rinsed with 0.1 M sodium cacodylate buffer (pH 7.0). The specimens were post-fixed in 1% osmium tetroxide in cacodylate buffer for 2 h. They were then dehydrated in ascending grades of ethyl alcohol and embedded in epoxy resin, followed by ultrathin and observation using a transmission electron microscope (JEM-1400; JEOL Co., Ltd., Tokyo).

RESULTS

The results of this study are summarized in Table 2 and shown in Figures 1–6.

Control group

To compare normal and ABMR renal biopsies, we observed renal transplant intraoperative 0-h biopsies by LVSEM as a control group. On LVSEM, PAM-stained positive GBMs, Bowman capsule's basement membrane, and the PTC basement membrane were observed clearly with bright appearances when contrasted with PAM-negative podocytes and endothelial cells, which were barely observed. Figure 1a–d shows LM and LVSEM images of a glomerulus in 0-h biopsies. In the control group, duplication of the GBM was not found in both PAM-stained LM and LVSEM images. Under LVSEM, the GBM was generally found to be faint and smooth. The three-dimensional ultrastructural changes of the GBM from both the capillary lumen and urinary space sides were examined in detail. The surface of the GBM on the capillary lumen side had a smooth and fine surface in the control group. Figure 1e and 1f presents LVSEM images of PTC in the control group. On LVSEM, PTC basement membranes were PAM-stained and observed clearly with bright appearances. Its basement membrane was found to be faint and smooth in the control group.

ABMR group — duplication of the GBM

Figure 2a–f shows LM and LVSEM images of glomeruli in the ABMR group (ABMR-6) following

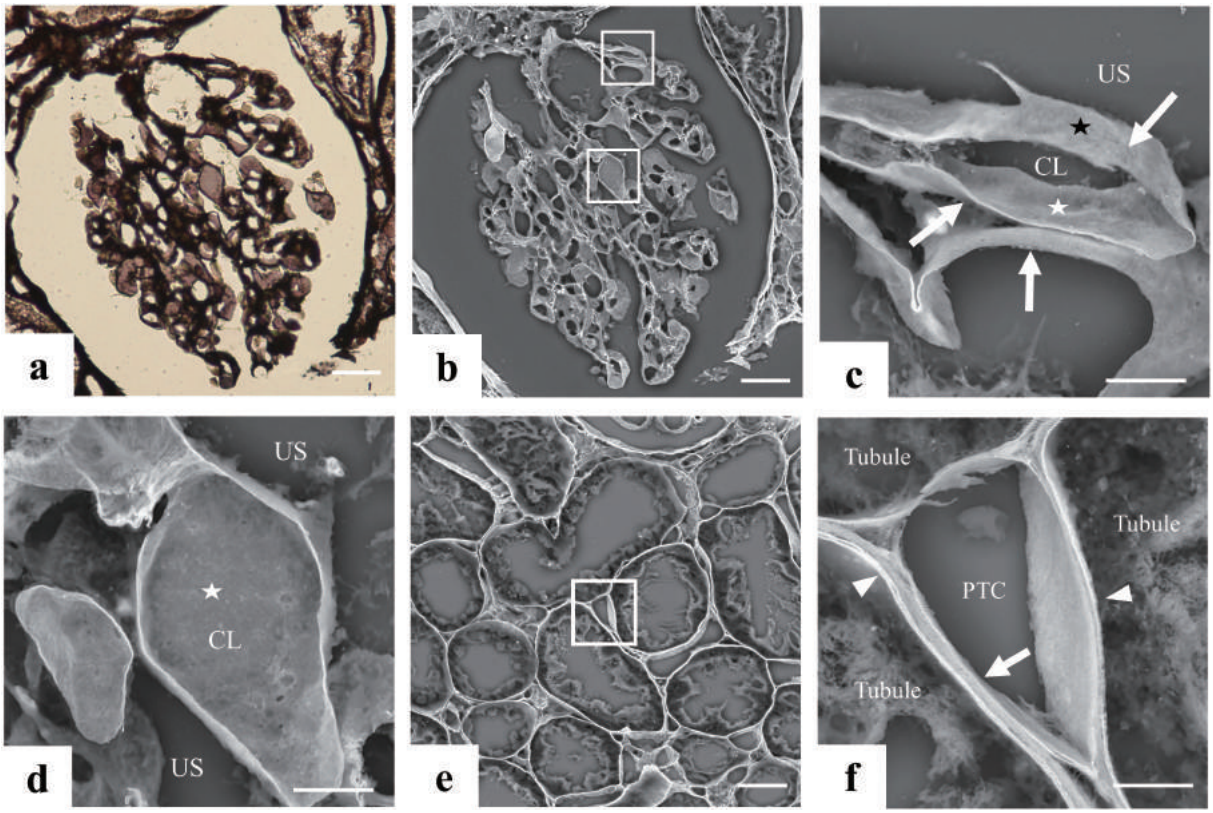

Fig. 1 LM (a) and LVSEM (b, c, d) images of a glomerulus, and LVSEM images of PTC (e, f) in intraoperative 0-h biopsy samples (control-2) stained with PAM. (**a**) LM image of a glomerulus (direct magnification, ×400). (**b**) Three-dimensional cut surface view of the same glomerulus (×600). (**c**) Higher-magnification image (×5000) of the upper square shown in (b). The GBMs (arrows) are thin and smooth. Three-dimensional structural imaging enabled the observation of both the urinary space side (black star) and capillary lumen side (white star) of the GBM surface. (**d**) Higher-magnification image (×5000) of the lower square shown in (b). The surface of the GBM on the capillary lumen side (white star) is smooth. (**e**) Renal PTC among renal tubules in the cortex (×600). (**f**) Higher-magnification image (×5000) of the square shown in (e). The basement membrane of the PTC (arrow) is thin and smooth. The arrowheads indicate the basement membrane of tubules. CL: capillary lumen, US: urinary space. Bars: 20 μm (a, b, e), 5 μm (c, d, f).

PAM staining. Duplication of the GBM was more clearly visible in the LVSEM images than in the LM images. There were sections in which duplication of the GBM was visible on LVSEM, but not on LM. This sample was scored as cg2 using LM but as cg3 using LVSEM. Even in the same LVSEM observations, there were regions in which duplication of the GBM could be judged only at high magnification (Fig. 2c). Figure 3 shows LM and LVSEM images of early ABMR (ABMR2-2) following PAM staining. In this specimen, duplication of the GBM was not seen using LM, and thus the specimen was scored as cg0. However, on LVSEM, clear duplication of the basement membrane was observed in multiple glomeruli, and the specimen was scored as cgla. Figure 4 shows a summary of the biopsy time course of case ABMR2. TG was first indicated by LM at 20 months in this case. However, in this research, duplication of the GBM was indicated using LVSEM even in 9- and 14-months samples. Thus, among the cases with repeated biopsies, three cases (ABMR2, ABMR3, ABMR4) exhibited duplication of the GBM in samples analyzed by LVSEM, but not by LM, at an earlier biopsy time (ABMR2-1, ABMR2-2, ABMR3-2, and ABMR4-1). In the 13 samples from the ABMR group, the cg score of the Banff classification was higher in 54 % (7/13) of cases for LVSEM images than for LM images.

ABMR group — PTC

On LVSEM observations in the ABMR group, thickening and a meshwork structure of the basement membrane of PTC were found on PAM staining compared to control group (Fig. 5).

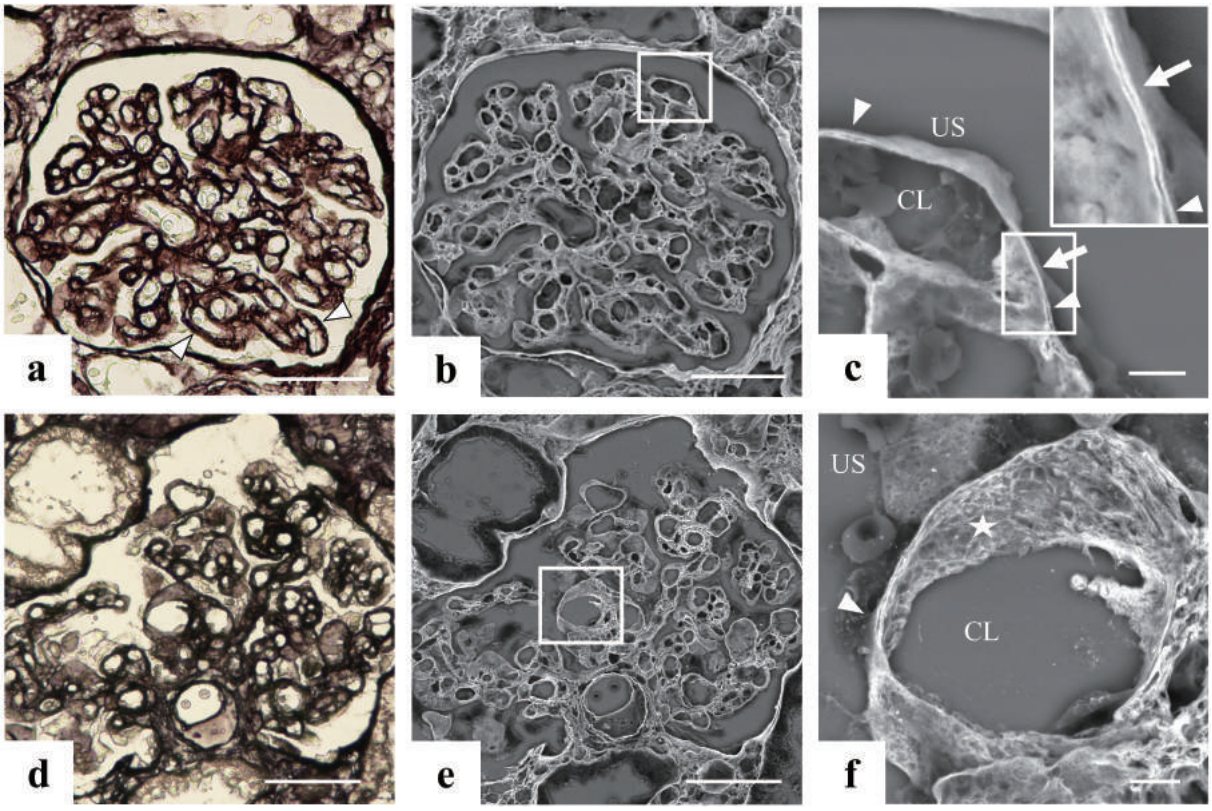

Fig. 2 Renal glomeruli stained with PAM in a case of severe ABMR (ABMR6). LM (a, d) and LVSEM images (b, c, e, f) are shown. (**a**) Some duplications of the GBM are visible on LM in this glomerulus (white arrowheads) (×400). (**b**) LVSEM image of the same glomerulus (×400). (**c**) Higher-magnification image (×2000) of the square shown in (b). The duplication of the GBM is clearly visible (arrowheads). On the other hand, the duplication of the GBM is not visible at the site denoted by arrow at this magnification. The inset shows a higher-magnification image (×5000) of the area captured by the square. The duplication of the GBM in the area indicated by the arrow is barely visible at this high-magnification. (**d**) LM image of another glomerulus in same specimen (×400). (**e**) LVSEM image of the glomerulus shown in (d) (×400). (**f**) Higher-magnification image (×3000) of the square shown in (e). The duplication of the GBM is observed (arrowhead). Coarse meshwork structures are present on the GBM surface on the capillary lumen side (star). CL: capillary lumen, US: urinary space. Bars: 50 μm (a, b, d, e), 5 μm (c, f).

ABMR group — other ultrastructural changes

In ABMR specimens, characteristic three-dimensional ultrastructural changes in GBM were also observed with LVSEM. Coarse meshwork structures were frequently found on the external side of GBM in the ABMR group (Figs. 2f, 3c). The coarse meshwork structure on the surface of the GBM tended to be remarkable in cases of GBM duplication. Similarly, small pouch-like shapes were also observed in the GBM of the ABMR cases (Fig. 3e, f). These three-dimensional ultrastructural changes were visible on LVSEM but not on LM. Almost none of these distinctive findings was observed in the control group.

Figure 6a–c shows TEM images of two specimens observed by the re-embedding method (ABMR2-2 and ABMR3-3). In these two specimens, GBM duplication was not observed on LM, whereas it was visible on LVSEM. On TEM observations, duplication of the GBM was found in both cases. TEM also uncovered the multilayering of five or more layers of the basement membranes of PTCs.

DISCUSSION

In this study, cases of ABMR following renal transplantation were analyzed using LVSEM. LVSEM allows the identification of GBM duplication and ultrastructural changes of basement membranes at the electron microscopic level in ABMR group.

To prolong graft survival, early diagnosis and treatment ABMR may help. Observation of ultrastructural changes in TG detected using electron microscopy, is important in diagnosing early-stage

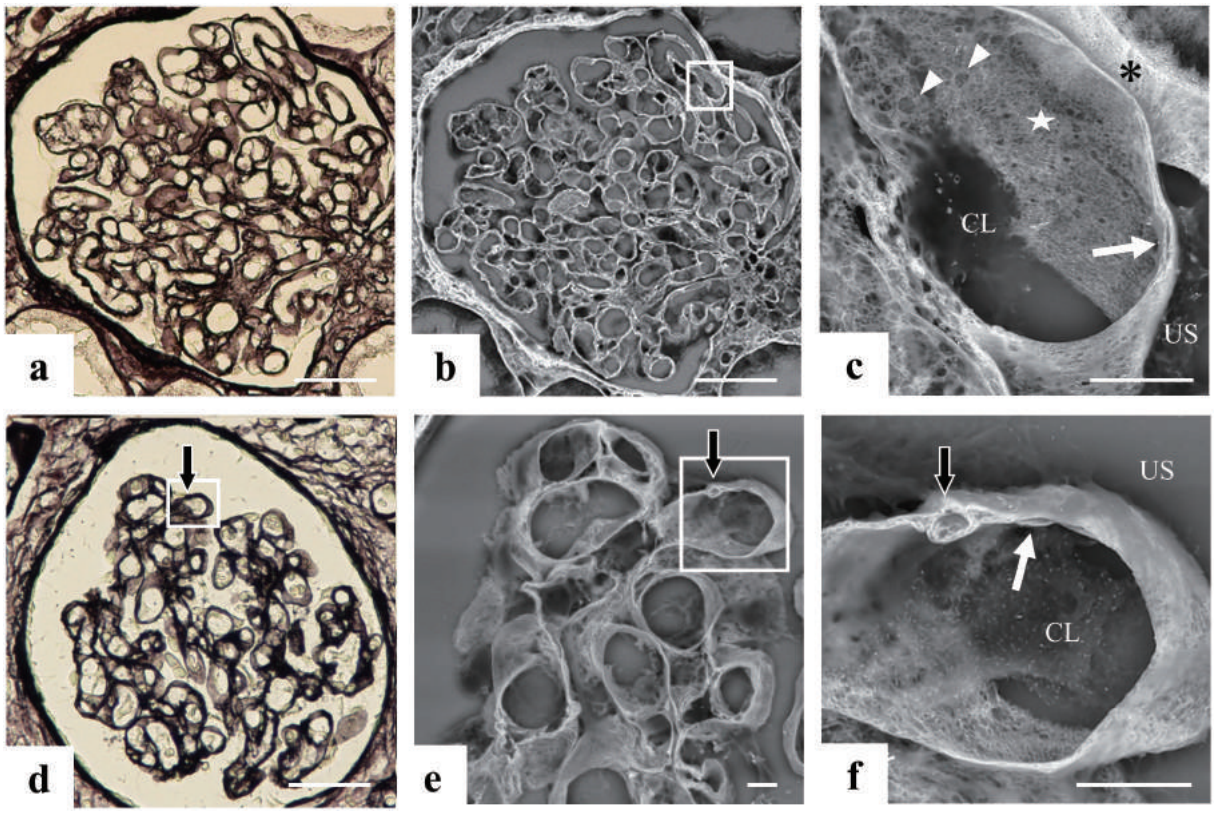

Fig. 3 Renal glomeruli in a case of early-stage ABMR (ABMR2-2). LM (a, d) and LVSEM (b, c, e, f) images of PAM-stained glomeruli are shown. (**a**) LM image of a glomerulus (×400). The duplication of the GBM is not visible using LM in this glomerulus. (**b**) LVSEM image of the same glomerulus shown in (a) (×400). (**c**) Higher-magnification image (×6000) of the square shown in (b). The duplication of the GBM is clearly visible (white arrow). Close to the glomerular capillary, Bowman's capsule is observed (asterisk). The capillary lumen side of the GBM surface (star) has a comparatively fine meshwork structure; however, some coarse meshwork structures are present (white arrowhead). (**d**) LM image of another glomerulus in same specimen (×400). The region denoted by the black arrow appears to be a simply thickened GBM on LM. (**e**) LVSEM image of the same glomerulus shown in (d) (×1500). (**f**) Higher-magnification image (×7000) of the square shown in (e). The duplication of the GBM is visible (white arrow). A "small pouch-like shape" is observed in the duplicated GBM (black arrow). CL: capillary lumen, US: urinary space. Bars: 50 μm (a, b, d), 5 μm (c, e, f).

ABMR (6, 21). Wavamunno *et al.* demonstrated that early GBM duplication detectable within the first 3 months after transplantation by TEM is correlated with the later development of overt TG (21). Haas *et al.* confirmed and extended these findings, demonstrating that early GBM duplication on TEM is highly associated with ABMR (6). However, TEM is costly and time consuming, and requires the collection of dedicated specimens at the time of the biopsy. Realistically, excluding some advanced facilities, use of TEM for every case of renal transplant biopsy is impossible. A report found that only 22% of laboratories always collected a sample from transplant biopsies for TEM (17). Moreover, the field of observation using TEM is limited, and the result may not be an accurate representation of the whole transplanted kidney. Another type of electron microscopy, conventional scanning electron microscope (SEM), also requires specialized technology and is expensive. Moreover, analyzing the GBM by conventional SEM using secondary electron signals requires further special and complicated processing, such as the removal of epithelial and endothelial cells (1, 2).

Contrarily, LVSEM has many remarkable advantages compared with TEM and conventional SEM (11). LVSEM is simple and easy to use, is comparatively less expensive, and permits convenient and quick observations. LVSEM can be used to obtain high-magnification images using conventional paraffin sections for any part of interest within the section, even with a previously collected specimen. Combining LVSEM with metal staining allows the characteristic three-dimensional imaging of the renal

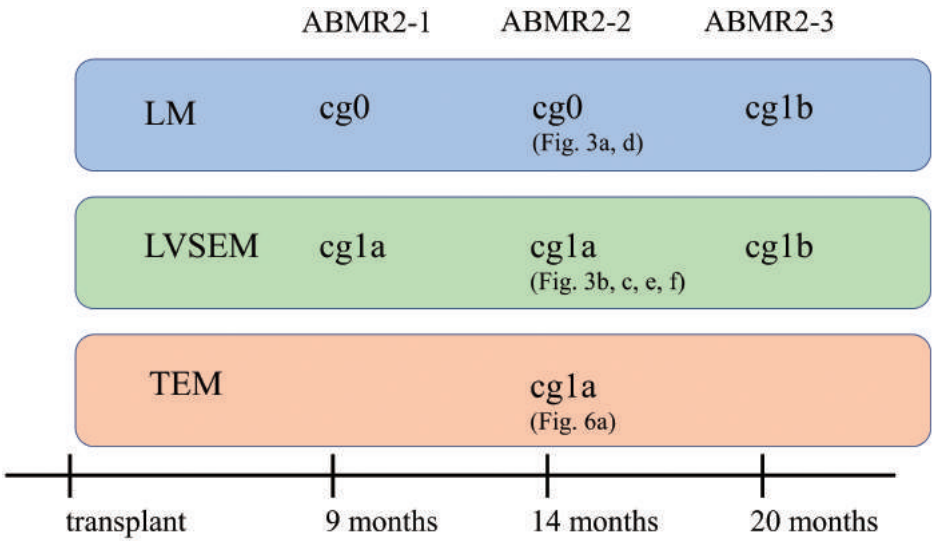

Fig. 4 Summary of biopsy time course of case ABMR2. Cg score using LM, LVSEM, and TEM in this study.

tissue in BSE mode. With PAM staining, which is routine in renal pathology, the basement membrane is stained, but not the endothelial and epithelial cells. Therefore PAM-positive basement membrane, which yield much BSE signals, is distinctly detected through PAM-negative overlying cellular elements under LVSEM. Thus, unlike conventional SEM, LVSEM does not require the removal of endothelial and epithelial cells before observing the basement membrane itself. The contrasts between the GBMs and cellular components contributed to the clear observations of GBMs on LVSEM. It excelled in three-dimensional structural imaging, and the system was adapted at visualizing duplicated GBMs and their gaps.

In this study, cases of ABMR following renal transplantation were analyzed using LVSEM, which more clearly revealed GBM duplication than LM. The absence of GBM duplication in the control group on LVSEM suggests that this technique is associated with a low probability of false positives regarding basement membrane duplication. The TEM findings confirmed the absence of contradictions between the ABMR diagnoses and LVSEM findings. This finding demonstrated the potential use of LVSEM in identifying TG and thus in diagnosing ABMR in renal transplant recipients in accordance with the present Banff classification. The presence of glomerular capillary remodeling alone is not pathognomonic in TG. Duplication of GBMs is also observed in recurrent membranoproliferative glomerulonephritis, hepatitis C virus infection, and thrombotic microangiopathy in renal allografts (4, 9). However, the LM findings and medical records did not suggest these conditions in this study.

Similar to the glomerular capillary, endothelial cell activation and damage with basement membrane changes occur in PTCs (13). Each ring of the basement membrane surrounding a PTC probably represents the residue of one previous episode of endothelial injury, starting from the oldest to the most recent (19). PTC lamination is correlated with TG and ABMR diagnoses (7). In this study, thickening and the meshwork structure of the PTC basement membranes were observable in the ABMR group using LVSEM. However, quantitative evaluation of PTC basement membrane multilayering with LVSEM could not be performed. TEM provides two-dimensional sectioned images of specimens, clearly indicating the changes in the layers. Conversely, LVSEM provides three-dimensional images including deep BSE signals, making it difficult to count the layers of the basement membranes. Further comparative studies with TEM are needed.

In this study, LVSEM often revealed characteristic three-dimensional ultrastructural changes such as a “coarse meshwork structure” and a “small pouch-like shape” in GBMs in the ABMR group. To the best of our knowledge, no prior reports revealed these types of pathological findings using LM or TEM. A previous study observed acellular GBM using SEM, and normal GBM was stated to be externally smooth and thin (1, 2). Bonsib and others have, in terms of cases of glomerulonephritis, observed irregular cavities and craters of various sizes on the surface of the GBM in their SEM observa-

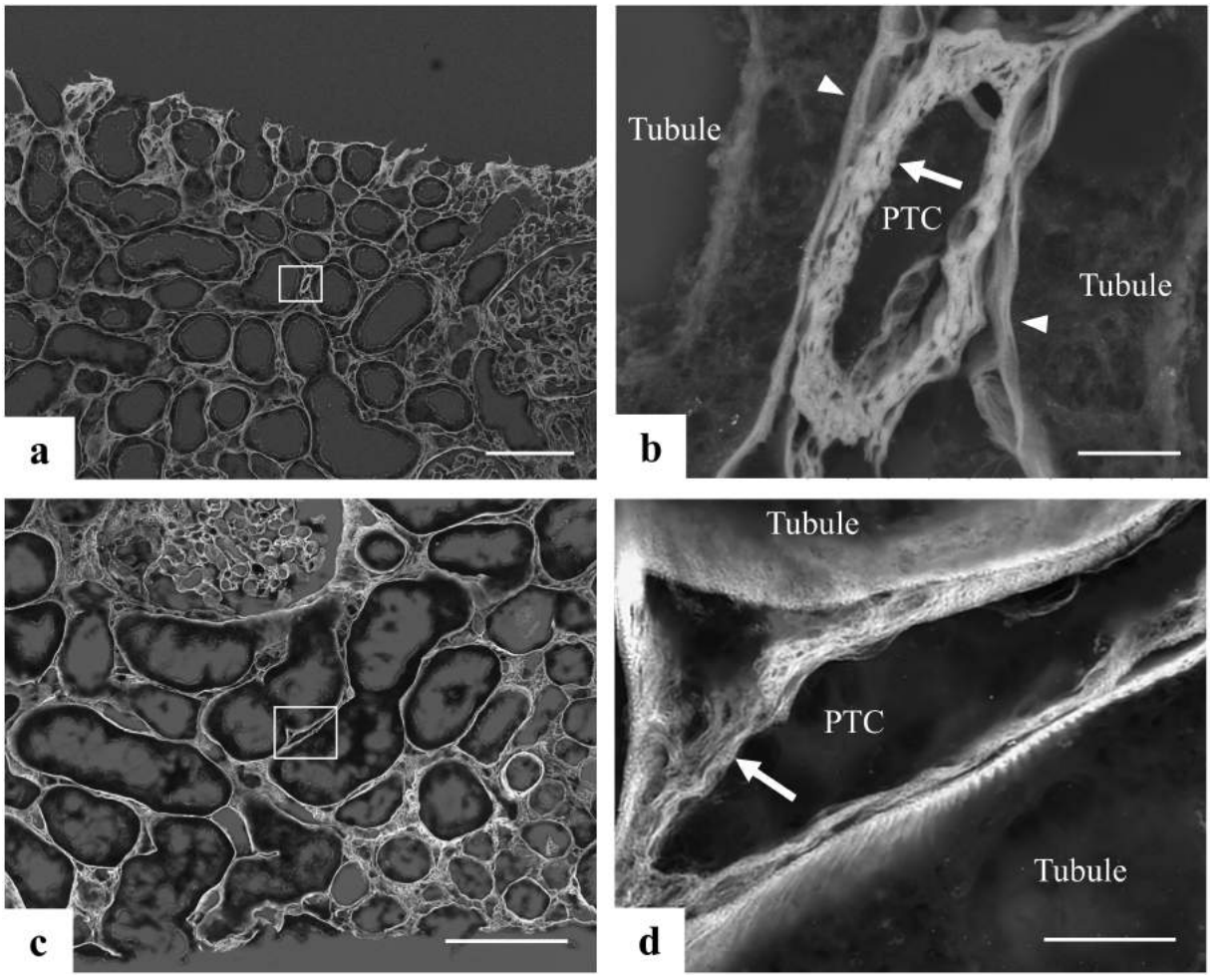

Fig. 5 LVSEM images of renal PTC stained with PAM in a case of severe ABMR (ABMR6). (**a**) Renal PTC among renal tubules (×200). (**b**) Higher-magnification image (×5000) of the square shown in (a). Thickening and the meshwork structure of the basement membrane are observed (arrow). The arrowhead indicates the basement membrane of tubules. (**c**) Another renal PTC among renal tubules (×300). (**d**) Higher-magnification image (×7000) of the square shown in (c). Thickening and the meshwork structure of the basement membrane are observed (arrow). Bars: 100 μm (a, c), 5 μm (b, d).

tions, and they surmised that these findings denote an "immune complex-mediated glomerular injury" (1). The findings of the basement membrane presented in their report are similar to the coarse meshwork structures revealed by LVSEM in this research. The coarse meshwork structure of the external side of GBM may be one of the changes of basement membrane induced by chronic endothelial cell dysfunction. The significance of the "small pouch-like shape" changes observed in the GBM of the ABMR group is unknown at present. It might be three-dimensional ultrastructural change caused by GBM damage.

This study had several limitations. Other than the duplication of the GBM and PTC basement membrane multilayering, the changes of the endothelial cells of glomerular capillaries and PTCs are important as pathological changes of early-stage ABMR (3, 6, 21). TEM revealed glomerular endothelial swelling, loss of fenestrations, and subendothelial electron-lucent widening as important early-stage ABMR findings. The cg evaluation in this research assessed only the duplication of the basement membrane, but fundamentally, observing the changes of endothelial cells is also necessary. We were, however, unable to evaluate such changes in this study. Endothelial cells could not be examined because they are PAM-negative elements. Meanwhile, we previously developed the Pt-blue staining method to reveal the morphological changes of glomerular cellular components under LVSEM (10, 11, 15). We hope that further studies will be performed in the future to address

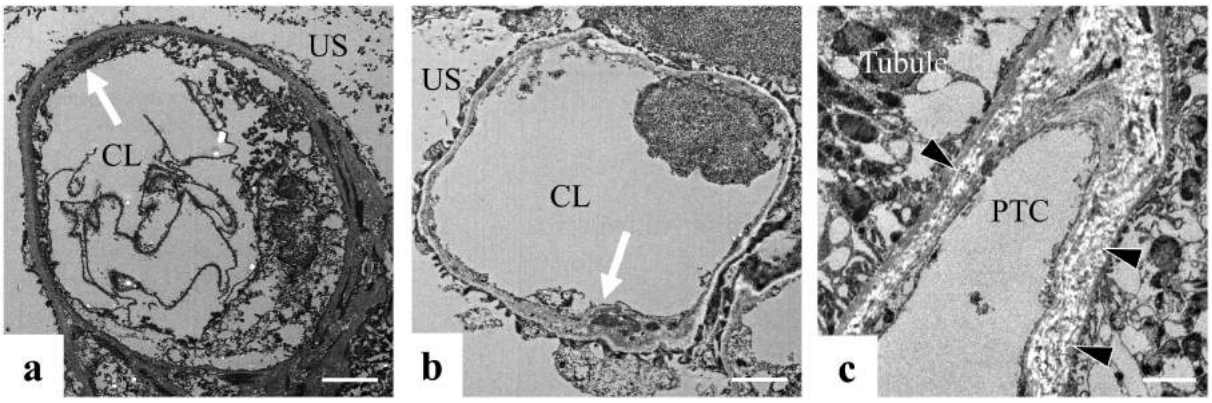

Fig. 6 TEM images of two samples in the ABMR group analyzed using the re-embedding method. (**a**) TEM image of the glomerulus of the same sample used in Figure 2 (ABMR2-2) (×4000). The duplication of the GBM is also visible on TEM (white arrow). (**b**) TEM image of another glomerulus (×4000) (ABMR3-2). The duplication of the GBM is observed (white arrow). (**c**) TEM image of a part of PTC (×1500) (ABMR3-2). Multilayering is observed in PTC basement membranes (black arrowheads). CL: capillary lumen, US: urinary space. Bars: 2 μm (a, b, c).

these issues. In addition, the number of cases was rather limited, and the study was retrospective, making generalization of the results difficult.

In conclusion, cases of ABMR following renal transplantation were analyzed using LVSEM, and the duplication of the GBM was observed more clearly using LVSEM than using LM. LVSEM can potentially be useful for the early diagnosis of ABMR.

Acknowledgements

The authors are grateful to Dr. Hisao Ito, professor emeritus of Tottori University, for providing pathological specimens, Dr. Kazuhiko Hayashi professor in Tottori University, for his assistance in this study; and Mr. Toshio Kameie, Mr. Norihisa Itaki, and Mr. Takashi Horie, Tottori University, for their technical supports.

REFERENCES

1. Bonsib SM (1985) Scanning electron microscopy of acellular glomeruli in nephrotic syndrome. *Kidney Int* **27**, 678–684.
2. Carlson E (1994) Scanning and transmission electron microscopic studies of normal and diabetic acellular glomerular and retinal microvessel basement membranes. *Microsc Res Tech* **28**, 165–177.
3. Drachenberg C and Papadimitriou J (2013) Endothelial injury in renal antibody-mediated allograft rejection: A schematic view based on pathogenesis. *Transplantation* **95**, 1073–1083.
4. Filippone EJ, McCue PA and Farber JL (2018) Transplant glomerulopathy. *Mod Pathol* **31**, 235–252.
5. Gosset C, Lefaucheur C and Glotz D (2014) New insights in antibody-mediated rejection. *Curr Opin Nephrol Hypertens* **23**, 597–604.
6. Haas M and Mirocha J (2011) Early ultrastructural changes in renal allografts: Correlation with antibody-mediated rejection and transplant glomerulopathy. *Am J Transplant* **11**, 2123–2131.
7. Haas M, Sis B, Racusen L, Solez K, Glotz D, Colvin R, *et al.* (2014) Banff 2013 Meeting Report: Inclusion of C4d-negative antibody-mediated rejection and antibody-associated arterial lesions. *Am J Transplant* **14**, 272–283.
8. Haas M, Mirocha J, Reinsmoen NL, Vo AA, Choi J, Kahwaji JM, *et al.* (2017) Differences in pathologic features and graft outcomes in antibody-mediated rejection of renal allografts due to persistent/recurrent versus de novo donor-specific antibodies. *Kidney Int* **91**, 729–737.
9. Hara S (2017) Current pathological perspectives on chronic rejection in renal allografts. *Clin Exp Nephrol* **21**, 943–951.
10. Inaga S, Hirashima S, Tanaka K, Katsumoto T, Kameie T, Nakane H, *et al.* (2009) Low vacuum scanning electron microscopy for paraffin sections utilizing the differential stainability of cells and tissues with platinum blue. *Arch Histol Cytol* **72**, 101–106.
11. Inaga S, Kato M, Hirashima S, Munemura C, Okada S, Kameie T, *et al.* (2010) Rapid three-dimensional analysis of renal biopsy sections by low vacuum scanning electron microscopy. *Arch Histol Cytol* **73**, 113–125.
12. Ivanyi B, Kemeny E, Szederkenyi E, Marofka F and Szenohradszky P (2001) The value of electron microscopy in the diagnosis of chronic renal allograft rejection. *Mod Pathol* **14**, 1200–1208.
13. Lipták P, Kemény É, Morvay Z, Szederkényi E, Szenohradszky P, *et al.* (2005) Peritubular capillary damage in acute humoral rejection: An ultrastructural study on human renal allografts. *Am J Transplant* **5**, 2870–2876.
14. Loupy A, Haas M, Solez K, Racusen L, Glotz D, *et al.* (2017) The Banff 2015 Kidney Meeting Report: Current challenges in rejection classification and prospects for adopting molecular pathology. *Am J Transplant* **17**, 28–41.
15. Okada S, Inaga S, Kawaba Y, Hanada T, Hayashi A, Nakane H, *et al.* (2014) A novel approach to the histological diagnosis of pediatric nephrotic syndrome by low vacuum scanning electron microscopy. *Biomed Res (Tokyo)* **35**, 227–236.
16. Okada S, Inaga S, Kitamoto K, Kawaba Y, Nakane H, Naguro T, *et al.* (2014) Morphological diagnosis of Alport syndrome and thin basement membrane nephropathy by low

vacuum scanning electron microscopy. *Biomed Res (Tokyo)* **35**, 345–50.
17. Pullman JM, Ferrario F and Nast CC (2007) Actual practices in nephropathology: a survey and comparison with best practices. *Adv Anat Pathol* **14**, 132–140.
18. Remport A, Ivanyi B, Mathe Z, Tinckam K, Mucsi I and Molnar MZ (2015) Better understanding of transplant glomerulopathy secondary to chronic antibody-mediated rejection. *Nephrol Dial Transplant* **30**, 1825–1833.
19. Roufosse C, Shore I, Moss J, Moran L, Willicombe M, Galliford J, *et al.* (2012) Peritubular capillary basement membrane multilayering on electron microscopy: A useful marker of early chronic antibody-mediated damage. *Transplantation* **94**, 269–274.
20. Stegall M, Diwan T, Raghavaiah S, Cornell L, Burns J, Dean P, *et al.* (2011) Terminal complement inhibition decreases antibody-mediated rejection in sensitized renal transplant recipients. *Am J Transplant* **11**, 2405–2413.
21. Wavamunno MD, O'Connell PJ, Vitalone M, Fung CL-S, Allen RDM, Chapman JR, *et al.* (2007) Transplant glomerulopathy: Ultrastructural abnormalities occur early in longitudinal analysis of protocol biopsies. *Am J Transplant* **7**, 2757–2768.